Energy Scales of Compositional Disorder in Alloy Semiconductors

Sergei D. Baranovskii,* Alexey V. Nenashev,* Dirk Hertel, Florian Gebhard, and Klaus Meerholz

Read Online

ACCESS | Metrics & More | Article Recommendations

ABSTRACT: The study of semiconductor alloys is currently experiencing a renaissance. Alloying is often used to tune the material properties desired for device applications. It allows, for instance, to vary in broad ranges the band gaps responsible for the light absorption and light emission spectra of the materials. The price for this tunability is the extra disorder caused by alloying. In this mini-review, we address the features of the unavoidable disorder caused by statistical fluctuations of the alloy composition along the device. Combinations of material parameters responsible for the alloy disorder are revealed, based solely on the physical dimensions of the input parameters. Theoretical estimates for the energy scales of the disorder landscape are given separately for several kinds of alloys desired for applications in modern optoelectronics. Among these are perovskites, transition-metal dichalcogenide monolayers, and organic semiconductor blends. While theoretical estimates for perovskites and inorganic monolayers are compatible with experimental data, such a comparison is rather controversial for organic blends, indicating that more research is needed in the latter case.
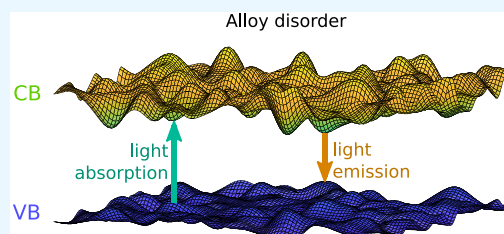
1. INTRODUCTION

Semiconductors are the basis of devices used in modern optoelectronics. They play a vital role in computing, communications, photovoltaics, sensing, and light emission. Alloying semiconductors is one of the most efficient tools to adjust material properties to the demands of particular device applications. For instance, alloys of III−V semiconductors, such as $Al_xGa_{1-x}As$, are used on an industrial basis for the manufacturing of semiconductor lasers, such as quantum well lasers, quantum cascade lasers, vertical-cavity surface-emitting lasers, etc. Particularly, quantum well lasers are the basic active element of the Internet fiber optic communication.

Mixing several semiconducting materials as an alloy allows one to tune lattice constants, effective masses of charge carriers, and most importantly, the band structure of the underlying materials. Particularly, band gaps in the alloy semiconductors are sensitive to the mole fractions of the alloy components. Since the band gap, E_g, is a key property responsible for light absorption and light emission, the opportunity to tune E_g in a wide energy range opens up rich prospects for applications of alloy semiconductors in various optoelectronic devices: for instance, in solar cells and in light-emitting diodes (LEDs). Band gap engineering by alloying has a long tradition in semiconductor research. For instance, alloying wide-band-gap II−VI semiconductors, such as ZnSe and ZnTe, was used already in the 1990s, targeting applications in visible light-emitting devices in the blue-green region. In Figure 1 the composition dependence of the band gap in the alloy $ZnSe_xTe_{1-x}$ is plotted in order to illustrate the effect of the band-gap engineering.[1] Varying the composition x in this alloy, one can vary the band gap in a broad range between $E_g(0.35) \simeq 2.2$ eV and $E_g(1) \simeq 2.8$ eV.
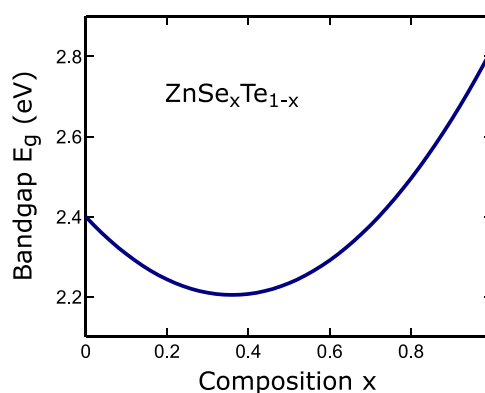
Figure 1. Composition dependence of the band gap in $ZnSe_xTe_{1-x}$. Adapted with permission from ref 1. Copyright 1993 by the American Physical Society.

In recent years, band-gap engineering has been applied to nitride semiconductors used in modern LEDs,[2] to perovskites for applications in photovoltaics,[3] to 2D systems, such as transition-metal dichalcogenides (TMDs), desired to miniaturize the corresponding devices toward nearly atomically thin dimensions,[4] and to organic disordered semiconductors[5] for

applications in organic light-emitting diodes (OLEDs), organic thin-film transistors (OTFTs), and organic solar cells (OSCs).[5,6]

The tunability of the semiconductor properties by alloying, however, has its price. Alloying always creates disorder, which affects the behavior of electrons and holes, causing spatial localization of charge carriers. Disorder effects are unfavorable for the device performance. Therefore, a control of the disorder effects is of vital importance for device applications of alloy semiconductors. Alloying can cause disorder in various forms. For instance, a mismatch in bond lengths caused by an ionic size discrepancy between the alloy components can cause elastic stress, contributing to the disorder potential. Another contribution to the disorder potential can be caused by uncontrolled clustering of alloy components. Moreover, in the case of perovskites, extra disorder can be caused by oxidation of alloy components and by vacancy formation. Additionally, the rapid crystallization rate often used in the manufacturing of alloy polycrystalline thin films can cause poor crystallinity and high spatial heterogeneity including crystallographic distortions (i.e., small grains and pinholes). In the case of TMDs, disordered atomic configurations are often reported in electron microscopy studies. Furthermore, due to their high surface to volume ratio in monolayers, the 2D materials suffer from additional sources of disorder introduced by the substrate roughness, impurities, and adsorbates above or below the monolayer.[4]

Disorder created by structural imperfections can in many cases be eliminated by optimization of the material growth conditions. However, there is a particular mechanism of disorder in alloys that cannot be eliminated by technological progress. It is the so-called compositional or alloy disorder, which arises due to statistical fluctuations in the spatial distributions of atoms and molecules belonging to the chemically different alloy components. In our mini-review, only this unavoidable compositional disorder is considered becuase it is always present in semiconductor alloys. The compositional statistical disorder puts a limit on the possible optimization of an alloy material aimed at diminishing the disorder effects. Being inherent for alloy materials, the compositional disorder is often called alloy disorder.

In order to introduce alloy disorder, let us consider, for simplicity, the binary alloy $A_x B_{1-x}$, whose lattice sites are occupied by A and B atoms with some average mole fraction (alloy composition) of A atoms equal to x. Due to purely statistical fluctuations of the alloy composition around the average value x, the local compositions of the alloy in different local volumes of the sample deviate from the average value x. This alloy disorder arises even in the most favorable case of the random distributions of the chemically different alloy components, A and B. The band edge of the conduction band, $E_c(x)$, and that of the valence band, $E_v(x)$, in semiconductor alloys depend on the alloy composition x. Therefore, statistical fluctuations of the local alloy composition around the average value x cause a disorder potential acting on electrons and holes, as illustrated in the figure in the abstract. The energy landscape caused by the disorder potential hinders the motion of charge carriers necessary for device performance. Furthermore, disorder creates band tails in the band gaps of alloys, as illustrated in Figure 2. Localization of charge carriers in the band tails significantly affects the optoelectronic properties of alloy semiconductors. The estimate of the energy amplitude of the alloy disorder ε_0 is one of the main goals of our mini-review.
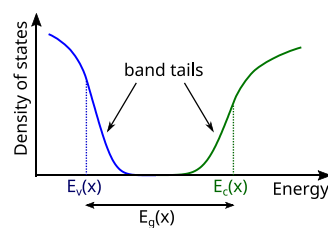
Figure 2. Schematic view of the density of states in disordered semiconductors.

Spatial fluctuations of $E_c(x)$ and $E_v(x)$ cause the spatial fluctuations of the band gap: $E_g(x) = E_c(x) - E_v(x)$. One of the most powerful tools for studying disorder effects in semiconductors is photoluminescence (PL). Fluctuations of $E_g(x)$ manifest themselves in the inhomogeneous broadening of the PL spectral lines. The inhomogeneous width of PL spectral lines δ_{PL} is, therefore, the quantity of primary interest to determine the strength of disorder effects. Disorder also causes energy differences between the absorption and PL emission spectra, called the Stokes shift. This difference arises due to the relaxation of the photoexcited charge carriers and excitons via the band-tail states. The magnitudes of the inhomogeneous PL line width, δ_{PL}, and that of the Stokes shift, Δ_{PL}, are the most used experimental tools to get access to the features of disorder potential in semiconductor alloys.[1,4,7,8] The origin of the PL inhomogeneous line width, δ_{PL}, and of the Stokes shift, Δ_{PL}, are schematically illustrated in Figure 3.
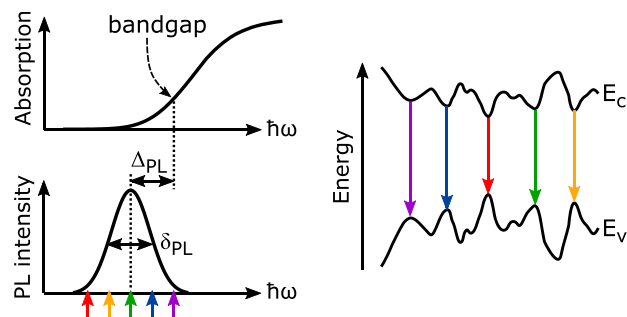


Figure 3. Schematic illustration for the origin of the PL inhomogeneous line width δ_{PL} and of the Stokes shift Δ_{PL}.

Particularly, the temperature dependences of $\delta_{PL}(T)$ and $\Delta_{PL}(T)$ have been proven useful to reveal the energy scale of disorder, ε_0, from a comparison between experimental data and theoretical simulations.[4,7−10] Following experimental studies,[3,11] we determine Δ_{PL} to be the difference between the absorption edge and the PL peak energy and determine δ_{PL} to be the full width at half-maximum of the PL spectral line. The typical temperature dependences of $\delta_{PL}(T)$ and $\Delta_{PL}(T)$ in disordered semiconductors are depicted in Figure 4.

There are two remarkable peculiarities with respect to the dependencies $\delta_{PL}(T)$ and $\Delta_{PL}(T)$ seen in Figure 4. One is the nonmonotonous temperature dependence of the Stokes shift $\Delta_{PL}(T)$. The other is the nonmonotoneous temperature dependence of the PL line width $\delta_{PL}(T)$. The mechanism of both effects is due to the exciton dynamics in the potential landscape created by disorder.[9]

Electrons and holes created by light absorption are bound in excitons, which are trapped into localized band-tail states. At very low $T \ll T_2$, excitons can move only toward localized states
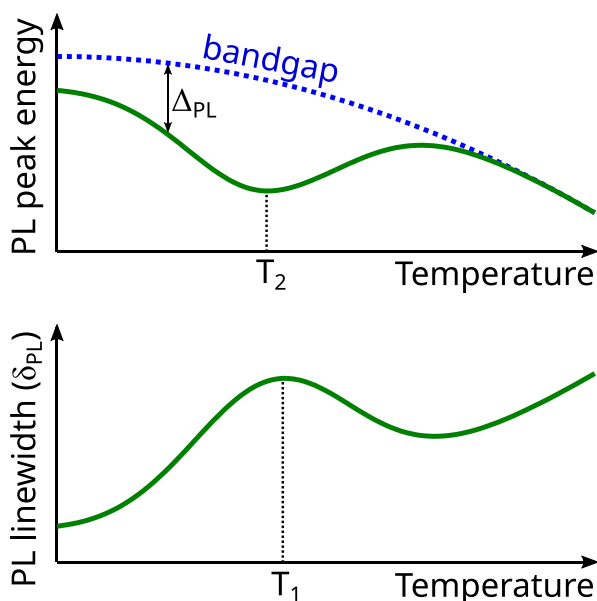
Figure 4. Typical temperature dependences of the PL peak energy and of the PL line width caused by the relaxation of photoexcited carriers via localized band-tail states. Adapted with permission from ref 7. Copyright 2010 by the American Physical Society.

with lower energies. This slow motion prevents excitons from achieving thermal equilibrium within their lifetime. The position of the PL peak corresponds to the energy depth in the band tails that can be achieved in this relaxation process within the exciton lifetime. With rising T, excitons can explore larger spatial regions within their lifetime, because the possibility of thermal activation enhances their mobility. As a consequence, the energy distribution of excitons counterintuitively shifts downward in energy with rising T and becomes closer to the equilibrium distribution. At $T \approx T_2$, the mobility of excitons becomes so high that the thermal distribution can be achieved within the exciton lifetime. At $T > T_2$ the PL spectrum is determined by the product between the density of states (DOS) in the band tail $g(\varepsilon)$ characterized by some energy scale ε_0 and the Fermi function $f(\varepsilon)$ characterized by the thermal energy kT, where k is the Boltzmann constant. The energy dependence of the DOS $g(\varepsilon)$ in disordered semiconductors is usually an exponential function or a steeper function.[1,4,7−9,12] Therefore, excitons at elevated temperatures are gathered in thermal equilibrium energetically close to the band edge. Therefore, the PL peak at $T \gg T_2$ follows the temperature dependence of the band gap (blue line in Figure 4). This causes the nonmonotonous dependence $\Delta_{PL}(T)$ depicted schematically in Figure 4.

The nonmonotonous temperature dependence of the PL line width $\delta_{PL}(T)$ is also due to the temperature-induced enhancement of the exciton mobility. At low T, excitons relax only downward in energy. Excitons in deep localized states relax more slowly than those in the shallow states. This leads to the compression of the exciton energy distribution, resulting in a narrow PL line width δ_{PL} at small $T < T_1$. At elevated temperatures, excitons become more mobile and can achieve thermal equilibrium. In such a situation, the exciton energy distribution is determined by the product $g(\varepsilon)f(\varepsilon)$. If the energy shape of the DOS $g(\varepsilon)$ is close to the exponential function, its product with the Fermi function is nearly constant at $kT_1 \approx \varepsilon_0$, yielding the broadest exciton energy distribution at $T = T_1$. At $T > T_1$, the energy distribution of excitons is narrower than that at

$T \approx T_1$ being prescribed by the energy scale of the DOS. At very high temperatures $T \gg T_1$, phonon effects come into play, causing a further increase of the PL line width.

Besides their unique properties favorable for device applications, alloy semiconductors are favorable systems for testing theoretical descriptions of disorder effects. The isoelectronic substitution of the alloy components creates a short-range fluctuating crystal potential. Therefore, the structure of the disorder potential is not complicated by the long-range effects, making it easy for theoretical treatments. The theoretical study of alloy disorder is currently experiencing a renaissance.[2] However, the effort of theoreticians in recent studies is focused mostly on the development of the theoretical algorithms for a description of the alloy potential. In this mini-review, we instead restrict the presentation of theory to elucidating the combinations of decisive semiconductor parameters responsible for the alloy disorder.

Avoiding elaborative calculations, the combinations of material parameters responsible for the energy amplitude and the spatial scale of alloy disorder are deduced in Section 2 from the general arguments based solely on the physical dimensions of the involved parameters. In Section 3, this theory is applied to various semiconductor alloys desired for device applications in modern optoelectronics. Concluding remarks are gathered in Section 4.

2. THEORETICAL DESCRIPTION OF ALLOY DISORDER

Our goal is to deduce the combination of material parameters responsible for the energy amplitude, ε_0, and for the spatial scale, R_0, of the alloy disorder. We consider for simplicity the binary alloy $A_x B_{1−x}$, where A and B atoms are randomly distributed over sites with spatial concentration N. The theoretical description of disorder effects in multicomponent alloys is slightly more elaborate.[13] A comprehensive theory of alloy disorder in binary alloys was developed in the 1960s[14] and 1970s[15] based on the concept of the optimal fluctuation. Interested readers can find the precise equations in the original literature[14,15] or in numerous review articles and edited books. We instead present below the derivation based solely on the physical dimensions of the involved material parameters.

The energy positions of the conduction band edge, $E_c(x)$, and of the valence band edge, $E_v(x)$ in alloys depend on the alloy composition x. These dependences lead to the composition dependence of the band gap, $E_g(x) = E_c(x) − E_v(x)$, which is used for tuning the light absorption and emission spectra of alloys. Let us consider for certainty the dependence $E_c(x)$ depicted schematically in Figure 5. In alloyed semiconductors, this dependence is not always linear in the whole range $0 \leq x \leq 1$, but it usually can be linearized in the vicinity of the alloy composition x.
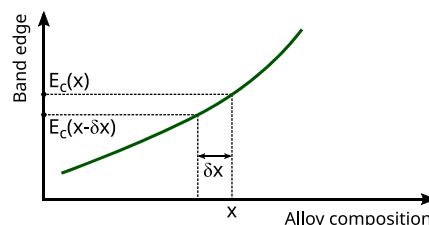
Figure 5. Schematic dependence of the conduction band edge $E_c(x)$ on the alloy composition x (solid line).

Consider a volume with a linear size R. The mean number of A atoms in this volume is on the order of xNR^3. In the case of Gaussian random statistical fluctuations, the typical excess number of A atoms in this volume is on the order of $\sim\sqrt{x(1-x)NR^3}$. The corresponding fluctuational change in the fraction of A atoms in the considered volume is on the order of

$$\delta x \simeq \frac{\sqrt{x(1-x)NR^3}}{NR^3} \qquad (1)$$

Since the position of the band edge E_c depends on the composition x, the band edge in the considered volume corresponds, at small fluctuations δx, to the energy

$$E_c(x, \delta x) = E_c(x) \pm \alpha_c \cdot \delta x \qquad (2)$$

where

$$\alpha_c = \left| \frac{dE_c(x)}{dx} \right| \qquad (3)$$

at $\delta x \to 0$. Thus, in the considered volume, a potential well (hump) is formed, with the depth (height)

$$V \simeq \alpha_c \frac{\sqrt{x(1-x)NR^3}}{NR^3} \qquad (4)$$

The potential energy V increases with decreasing size R of the considered volume. The choice of the appropriate value of R plays, therefore, the key role in the estimate of the energy scale of the alloy disorder.

In some cases, the physical problem already contains some characteristic length scale. For instance, donors and acceptors, imbedded into the alloy matrix, are characterized by the localization length of charge carriers, called the Bohr radius, $a_B = \hbar^2\kappa/me^2$, where $\hbar$ is the reduced Planck constant, e is the elementary charge, m is the effective mass of charge carriers, and κ is the dielectric constnt. Excitons created by light absorption are also characterized by a particular Bohr radius separating electrons and holes inside excitons. It looks tempting to insert a_B into eq 4 in order to estimate the characteristic energy scale of the alloy disorder. While such an action is justified in the case of immobile impurity atoms, it is not justified in the case of mobile excitons. Unfortunately, the latter has been overlooked in numerous frequently cited publications, where a_B was erroneously used as a characteristic space scale of the alloy disorder acting on excitons. In fact, excitons are affected by disorder acting on the exciton center of mass.[15] Therefore, one can consider excitons affected by the alloy disorder as quasi-particles with the mass $M = m_e + m_h$ equal to the sum of the electron and hole effective masses.[15] It appears to not be helpful to jump to conclusions using some prescribed length scale, such as , for instance, a Bohr radius of excitons. In order to avoid such errors, let us consider a single electron affected by the alloy disorder. The goal is to derive the energy scale ε_0 and the characteristic length $\tilde{R}$ of the alloy disorder affecting such an electron. The derivations will be carried out separately for three-dimensional (3D) and two-dimensional (2D) systems.

2.1. 3D Energy and Spatial Scales of the Alloy Disorder. The simplest derivation of ε_0 and $\tilde{R}$ looks as follows.[16] Only potential wells (not humps) can create localized states and contribute to the formation of band tails. If V and R satisfy the inequality $V \gg \hbar^2/mR^2$, such a well has a ground electron state close to $-V$. With the opposite inequality, the well

contains no electron states. According to eq 4, the depth of the well increases with decreasing R. Therefore, the most efficient wells are those with the smallest R, which yet contain bound electron states. Such potential wells are determined by the condition $V \simeq \hbar^2/m\tilde{R}^2$: i.e., $\tilde{R} \simeq (\hbar^4 N)/(\alpha^2 xm)$. Inserting this $\tilde{R}$ in eq 4 yields[16] the estimate for the characteristic scale of the alloy disorder $\varepsilon_0 \simeq (\alpha^4 x^2 m^3)/(\hbar^6 N^2)$. For the sake of generality, we replace α_c by α in eq 4, so that $\alpha = \alpha_c$ for the conduction band and $\alpha = \alpha_v$ for the valence band.

The precise combinations of material parameters for the energy scale, ε_0, and the spatial scale, R_0, of the alloy disorder can be deduced solely from the physical dimensions of the involved parameters.[15] When A and B atoms are randomly distributed, fluctuations $\delta x(r_1)$ and $\delta x(r_2)$ are statistically independent. In such a case, spatial fluctuations of the alloy composition create a random potential for electrons $V(r)$ in the form of a "white noise" with a negligibly small correlation length:

$$\langle V(r_1)V(r_2)\rangle = \gamma\delta(r_1 - r_2) \qquad (5)$$

with[17]

$$\gamma = \frac{\alpha^2}{N}x(1-x) \qquad (6)$$

Eigenstates of electrons in the fluctuating potential $V(r)$ are determined by the Hamiltonian

$$H = -\frac{\hbar^2}{2m}\Delta + V(r) \qquad (7)$$

Let us find out the combination of parameters entering eq 7, which yields a single parameter ε_0 with the physical dimension of energy, for instance, joule. There are only two parameters in eq 7: $\hbar^2/m$ present in eq 7 explicitly and $\gamma = \alpha^2 x(1-x)/N$ entering eq 7 via potential V, as determined by eq 5. The ratio $\hbar^2/m$ has the physical dimension J m^2, while parameter γ in 3D has the physical dimension J^2 m^3. The only possible expression for the energy scale ε_0 based on these two input parameters is

$$\varepsilon_0 = \left[\frac{\hbar^2}{m}\right]^\xi \cdot \gamma^\zeta \qquad (8)$$

with some numbers ξ and ζ. Since the left-hand side of eq 8 has the physical dimension joule, this equation means that the relation J$^\xi$ m$^{2\xi}$ J$^{2\zeta}$ m$^{3\zeta}$ = J should be fulfilled. The latter relation is only possible if $\xi = -3$ and $\zeta = 2$. Using these values of ξ and ζ and the value γ determined by eq 6, one comes from eq 8 to the result

$$\varepsilon_0 = \lambda\frac{\alpha^4 x^2(1-x)^2 m^3}{\hbar^6 N^2} \qquad (9)$$

A numerical factor λ is inserted into eq 9 because a derivation based solely on the physical dimensions of the input parameters, though elegant, cannot be responsible for numerical coefficients. We address the possible values of numerical parameter λ in the following sections.

The only spatial scale $\tilde{R}$ based on eqs 6 and 7 is to fulfill the relation

$$\tilde{R} = \left[\frac{\hbar^2}{m}\right]^\iota \cdot \gamma^\varpi \qquad (10)$$

with some numbers ι and ϖ. The right-hand side of eq 10 should possess a physical dimension of meter. It means that the relation

J^{ι} m$^{2\iota}$ $J^{2\varpi}$ m$^{3\varpi}$ = m should be fulfilled. This relation is only possible if ι = 2 and ϖ = −1. Inserting these numbers and γ determined by eq 6 into eq 10 yields the result

$$\tilde{R} = \frac{\hbar^4 N}{\alpha^2 x(1-x)m^2} \tag{11}$$

The combinations of alloy parameters in eqs 9 and 11 are in agreement with those obtained by much more elaborate theoretical tools: for instance, by the technique based on the optimal fluctuation approach.[14,15]

2.2. 2D Energy and Spatial Scales of the Alloy Disorder. The physical dimension of the ratio $\hbar^2/m$ in 2D is the same as in 3D, i.e., J m^2, while parameter γ has in 2D the physical dimension J^2 m^2. Using arguments analogous to those in Section 2.1, one comes in the 2D case to the only possible combinations of material parameters for the energy and spatial scales of the alloy disorder in the form

$$\varepsilon_0^{2D} = \frac{\alpha^2 x(1-x)m}{\hbar^2 N} \tag{12}$$

and

$$\tilde{R}^{2D} = \frac{\hbar^2 N^{0.5}}{|\alpha| x^{0.5}(1-x)^{0.5}m} \tag{13}$$

The combinations of alloy parameters in eqs 12 and 13 are in agreement with those based on the optimal fluctuation approach.[13]

3. ALLOY DISORDER IN VARIOUS SEMICONDUCTOR ALLOYS

In this section we apply theoretical estimates from Section 2 separately to several alloys desired for applications in modern optoelectronics. Perovskites, transition-metal dichalcogenide (TMD) monolayers, and organic semiconductor blends are addressed in the following subsections.

3.1. Alloy Disorder in Perovskites. Halide perovskite alloys are tremendously successful in photovoltaic and light-emitting applications.[18] For instance, perovskite/silicon tandem solar cells have reached 29% power conversion efficiency.[19] Most state-of-the-art perovskite solar cells use alloyed materials as absorber layers.[18] This is particularly the case for the all-perovskite tandem solar cells, in which compositional engineering is required to reach optimal band gaps to maximize efficiency.[18] For the sake of certainty, we focus our analysis on the mixed lead tin triiodide perovskites, which are promising absorber materials for low-band-gap bottom cells in all-perovskite tandem photovoltaic devices.[3,11,20] For instance, Figure 6 illustrates that the band gap in the perovskite alloy FAPb$_{0.4}$Sn$_{0.6}$I$_3$ is essentially narrower than that in each of the alloy components.[3] This figure represents, in fact, the data for the absorption edge at room temperature obtained by Parrott et al.[3] which we identify with the band gap, $E_g(x)$.

Discussing the effect of alloy disorder, we address below the experimental data in FAPb$_{1-x}$Sn$_x$I$_3$ and in FA$_{0.83}$Cs$_{0.17}$Pb$_{1-x}$Sn$_x$I$_3$ perovskite alloys obtained by Parrott et al.[3] and Savill et al.[11] The samples of the thin film alloys were obtained by spin-coating precursor solutions of FASnI$_3$ and FAPbI$_3$ in appropriate ratios.

As already stated in the Introduction, access to the features of disorder potential can generally be achieved by viewing the inhomogeneous PL line width δ_{PL} and the PL Stokes shift Δ_{PL}.[1,4,7,8,12] Studying δ_{PL} and Δ_{PL} in FAPb$_{1-x}$Sn$_x$I$_3$ and in
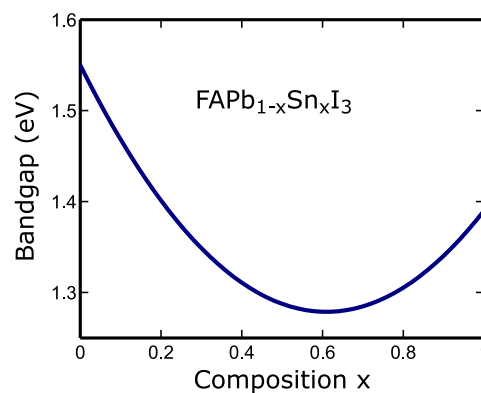
Figure 6. Composition dependence of the band gap in FAPb$_{1-x}$Sn$_x$I$_3$ perovskites at room temperature. Adapted with permission from ref 3. Copyright 2018 by Wiley.

FA$_{0.83}$Cs$_{0.17}$Pb$_{1-x}$Sn$_x$I$_3$ perovskites as a function of the lead:tin content, Parrott et al.[3] and Savill et al.[11] recognized that the 100% tin and 100% lead iodide perovskites have much sharper PL spectra and much smaller Stokes shifts than their alloys, indicating higher disorder for mixed-metal compositions. The data of Parrott et al.[3] for the line width δ_{PL} are reproduced in Figure 7.
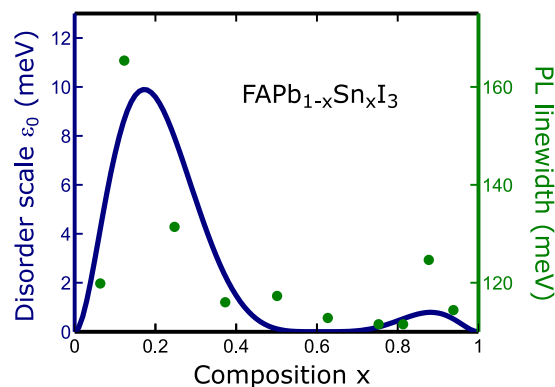
Figure 7. Solid line: dependence of the disorder energy scale $\varepsilon_0(x)$ on the composition x, as predicted by eqs 9, 14, and 15. Symbols: PL line width $\delta_{PL}(x)$ (fwhm) revealed experimentally. Adapted with permission from ref 3. Copyright 2018 by Wiley.

This observation was not considered surprising,[3,11] since the alloys are supposed to contain more disorder than the chemically pure alloy components. What, however, was treated as surprising[3] is the observation of the broadest PL line width and the largest Stokes shift in mixed compositions with Sn <25% and with >85%, while the largest effects of alloy disorder were intuitively expected for the 50:50 composition.[3] Therefore, it was concluded[3] that the revealed disorder effects might arise from extrinsic factors and can be eliminated upon further crystal growth optimization.

Using eq 9, we show below that the largest effects of alloy disorder are, in fact, expected for x_a < 0.25 and for x_b > 0.85. Moreover, the effect at x_a should be much more pronounced than that at x_b, in agreement with the experimental data.[3,11] Therefore, further crystal growth optimization might not be helpful to diminish the effects of alloy disorder in FAPb$_{1-x}$Sn$_x$I$_3$ and FA$_{0.83}$Cs$_{0.17}$Pb$_{1-x}$Sn$_x$I$_3$ perovskites.[21] In other words, the samples have already achieved a high quality with respect to the effects of alloy disorder.

If the parameters α, m, and N in eq 9 did not depend on x, $\varepsilon_0(x)$ would solely be proportional to $x^2(1-x)^2$ and would display a maximum at $x = 0.5$. This might be the reason the maximum disorder at $x = 0.5$ was intuitively expected in ref 3. However, it is unlikely that the parameter α in eq 9 did not depend on the composition x. This parameter plays a decisive role in converting the disorder in the spatial distribution of alloy components into the energy disorder described by eq 9.

The band gaps $E_g(x)$ in $FAPb_{1-x}Sn_xI_3$ and $FA_{0.83}Cs_{0.17}Pb_{1-x}Sn_xI_3$ evidence[3,11] strong dependences on the composition x at $x < 0.4$, and at $x > 0.8$ as depicted in Figure 6 for $FAPb_{1-x}Sn_xI_3$. The dependence, $E_g(x)$, is caused by the composition dependences of the band edges $E_c(x)$ and $E_v(x)$: $E_g(x) = E_c(x) - E_v(x)$. Observations of a strong x-dependent band gap[3,11] at $x < 0.4$ and at $x > 0.8$, $E_g(x)$, evidence that at least one of the band edges, $E_c(x)$ or $E_v(x)$, depends on the composition x at $x < 0.4$ and at $x > 0.8$. It is often the case in semiconductor alloys that only one of the band edges, $E_c(x)$, or $E_v(x)$, is responsible for the x dependence of the band gap, $E_g(x)$.[8] If it is $E_c(x)$, then parameter α in eq 9 is $\alpha_c = dE_c(x)/dx$, while the parameter $\alpha_v = dE_v(x)/dx$ can be neglected. In the opposite case when only $E_v(x)$ is responsible for the x dependence $E_g(x)$, the parameter α_c can be neglected and α in eq 9 is equal to $\alpha_v = dE_v(x)/dx$. In both such cases, α in eq 9 can be estimated as

$$\alpha = dE_g/dx \tag{14}$$

because $dE_g/dx = \alpha_c - \alpha_v$. Such an estimate of the parameter α in eq 9 via eq 14 is also often used in cases when the dependences $E_c(x)$ and $E_v(x)$ are not known, while the dependence $E_g(x)$ is measured, for instance, via the light absorption.[4] The validity of eq 14 for estimates of the energy disorder in mixed-metal lead tin triiodide perovskites is supported by the clear correlation between the magnitude of the parameter α determined by eq 14 and the luminescence line width δ_{PL}, reported recently in the experimental study by Klug et al.[20] (see Figure 4a,b in ref 20).

Studying the absorption edge, Parrott et al.[3] deduced the dependence $E_g(x)$ in the form

$$E_g(x) = xE_g^{Sn} + (1-x)E_g^{Pb} - x(1-x)b \tag{15}$$

with $b \simeq 0.73$, $E_g^{Pb} \simeq 1.55$ eV, and $E_g^{Sn} \simeq 1.39$ eV for the room-temperature phase. Let us use eqs 9, 14, and 15 in order to estimate the energy scale of disorder in the mixed tin lead triiodide perovskites. In Figure 7, the composition dependence $\varepsilon_0(x)$ in accord with these equations is plotted. In the calculations, a concentration of lattice sites $N = 4 \times 10^{21}$ cm^{-3} was used, based on the estimate for the lattice constant $a \simeq 6.3 \times 10^{-8}$ cm.[21] There is uncertainty in the choice of the effective mass m in eq 9. If electrons and holes appear in the form of excitons, the sum $m_e + m_h$ should be used. In the opposite case, either m_e or m_h should enter the equation. Since m_e and m_h in such perovskites are close to each other,[21] we use in eq 9, for the sake of certainty, the hole effective mass $m_h = 0.273m_0$.

Figure 7 shows that the energy scale of alloy disorder $\varepsilon_0(x)$ has two maxima at $x_a < 0.25$ and $x_b > 0.85$, in excellent agreement with the observations of Parrott et al.[3] for the x dependences of the luminescence line width δ_{PL} and of the luminescence Stokes shift Δ_{PL} as a function of the Sn concentration x.

In order to perform a quantitative fit of the PL line width $\delta_{PL}(x)$, it is necessary to possess a quantitative relation between the energy scale of disorder $\varepsilon_0(x)$ and the line width $\delta_{PL}(x)$. Computer simulations[7−10] show that this relation depends on

the DOS, $g(\varepsilon)$, in the band tails created by disorder potential. The shape of the DOS in the band tails of disordered semiconductors is usually described by an exponential function.[22] In the case of the conduction band tail, such a DOS reads

$$g(\varepsilon) = g(E_c) \exp\left(-\frac{E_c - \varepsilon}{\varepsilon_0}\right) \tag{16}$$

In the case of the exponential DOS, the relation between $\varepsilon_0(x)$ and $\delta_{PL}(x)$ in the broad range of material parameters reads for room temperature[10] $\delta_{PL}(x) \simeq 5\varepsilon_0(x)$. Therefore, the energy scale on the right y axis in Figure 7, where experimental data for $\delta_{PL}(x)$ are plotted, is enlarged by a factor of 5 as compared to the left y axis, where $\varepsilon_0(x)$ is shown. Furthermore, the value of the inhomogeneous line width $\delta_{PL}(0) \simeq \delta_{PL}(1) \simeq 110$ meV caused in the chemically pure alloy components at $x = 0$ and $x = 1$ by mechanisms other than the compositional disorder[3] is responsible for the origin of the energy on the right y axis. The quantitative agreement between the theoretical results based on eq 9 and experimental data are rather good. This good agreement without adjusting coefficients probably means that eq 9 is sufficient to determine the energy scale of the alloy disorder in perovskites without the numerical factor λ.

Most important is, however, not the quantitative agreement between the theoretical dependence $\varepsilon_0(x)$ and the experimental dependence $\delta_{PL}(x)$ based on several assumptions about the parameter values but rather the excellent agreement between the values $x_{a,b}$ for the maxima of the disorder energy scale $\varepsilon_0(x)$, as predicted by eq 9 and the Sn concentrations for the maximum disorder effects in the luminescence line width $\delta_{PL}(x)$ and in the Stokes shift $\Delta_{PL}(x)$, observed by Parrott et al.[3] and by Savill et al.[11]

These maxima of alloy disorder effects in mixed compositions with Sn fractions <25% and >85% could be one of the reasons Pb-rich and Sn-rich Sn−Pb perovskites typically show shorter PL lifetimes, broader emission, increased Stokes shifts, reduced PL quantum yields, and higher Urbach tails, compared with their lead-only counterparts.

3.2. Alloy Disorder in TMDs. Two-dimensional (2D) transition-metal dichalcogenides (TMDs) have currently attracted significant research interest because they are envisaged to play a crucial role in future high-tech devices.[4,23] TMDs have prospects in electronics, optoelectronics, and spintronics.[24] Furthermore, the monolayer crystal structure of TMDs has no inversion center, which enables charge carriers to have a new degree of freedom, the k-valley index. The manipulation of this index is envisaged for new applications in the field of valleytronics.[25]

TMDs are layered materials which combine a transition metal (M = Mo, W, Ti, Zr, etc.) and a chalcogen (X = S, Se, or Te) in the general formula MX_2 with one layer of M atoms sandwiched between two layers of X atoms. They are characterized by an intrinsic band gap within the visible and near-infrared regions. The band gaps in the TMD alloys can be tuned by varying the alloy composition in order to adjust the material properties to target specific applications. For instance, in the alloy $Mo_{1-x}W_xSe_2$ taken in this mini-review as an example of TMD alloys, the optical band gap can be continuously tuned from 1.45 eV (reached at $x = 0.21$) to 1.53 eV (reached at $x = 1$),[26] as illustrated in Figure 8. This dependence is described by the equation[26]

$$E_g(x) = 1.455 - 0.078x + 0.15x^2 \text{ eV} \qquad (17)$$
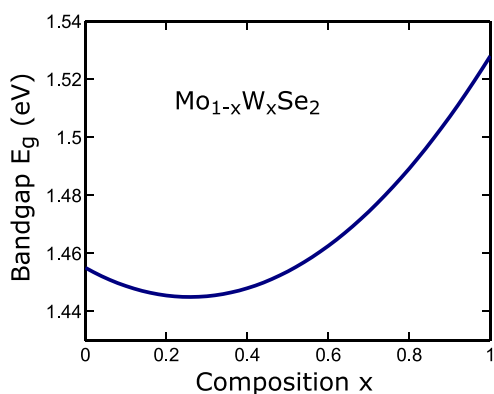
Figure 8. Composition dependence of the band gap in $Mo_{1−x}W_xSe_2$. Adapted with permission from ref 26. Copyright 2014 by the American Chemical Society.

Along with binary materials, MX_2, alloyed TMDs possess disorder caused by the substrate roughness, impurities, and adsorbates above or below the monolayer.[27] However, alloying causes an additional source of disorder due to spatial fluctuations of the disorder composition x. Similarly to the case of perovskites described in Section 3.1, it is important to reveal the dominant mechanism of disorder in TMDs in order to estimate the prospects for improvement of the device performance by crystal growth optimization. Recently, Masenda et al.[4] performed a systematic study of the statistical alloy disorder in $Mo_{1−x}W_xSe_2$ with $x = 0.7$. We present below selected results of this study. The samples were obtained by exfoliation of bulk crystals and transfer to polydimethylsiloxane. After identification of monolayers, a viscoelastic dry transfer method was employed to place the monolayers on pretransferred flakes of h-BN on a SiO_2/Si substrate using the same approach.

The situation with the TMDs appears similar to the case of perovskites described in Section 3.1: compositional fluctuations dominate the disorder effects. Due to the two-dimensional confinement of electrons and holes and the weak dielectric screening, excitons in TMD monolayers are stable even at room temperature and exhibit large binding energies of about 0.5 eV.[4] In order to address the features of the disorder potential in the atomically thin TMD $Mo_{1−x}W_xSe_2$, Masenda et al. experimentally studied the exciton photoluminescence in $Mo_{0.3}W_{0.7}Se_2$, comparing the features of the alloy monolayer with those of its binary counterparts, $MoSe_2$ and WSe_2. The measurements were carried out in a broad temperature range between 10 and 200 K. Particular attention was dedicated to the temperature dependences of the exciton PL Stokes shift Δ_{PL} and the PL line width $\delta_{PL}(T)$, which are known to be affected by the disorder potential, as proven in the literature for various well-studied 2D heterostructures manufactured from III–V and II–VI semiconductor materials.[7,9,10] In contrast to the binary materials, $MoSe_2$ and WSe_2, the alloy system demonstrates[4] nonmonotonous temperature dependences of the PL peak energy and of the line width, shown schematically in Figure 4. These features are known to be indicative of hopping-type relaxation of excitons via disorder-induced localized states in the band tails.[7−10,28] Results of computer simulations allow one to deduce the energy scale of the disorder potential from the temperature dependences of the PL peak energy and the PL line width.[7−10,28]

A comprehensive comparison of the temperature dependences $\Delta_{PL}(T)$ and $\delta_{PL}(T)$ measured by Masenda et al.[4] in the alloy monolayer $Mo_{0.3}W_{0.7}Se_2$ with those predicted by computer simulations[7−10,28] yielded[4] an energy scale of disorder potential in the range $6.5 \text{ meV} \leq \varepsilon_0 \leq 8.6 \text{ meV}$.

Let us compare this experimental estimate for the energy scale of disorder potential ε_0 in the 2D alloy monolayer with the theoretical prediction ε_0^{2D} given for 2D systems by eq 12 in Section 2.2. The equation can be applied to the PL features of excitons if the spatial scale of exciton localization is substantially larger than the exciton radius.[15] This condition is fulfilled for tightly bound excitons in TMDs with a very large exciton binding energy ($E_B \simeq 500 \text{ meV}$), as compared to the energy scale of disorder potential $\varepsilon_0 \approx 7 \text{ meV}$, estimated from the experiments.[4] In the case of excitons, the effective mass m is equal to the sum $m_e + m_h$ of the electron and hole effective masses.[15] Let us estimate the value of the parameter α via the variation of the optical band gap with the composition x depicted in Figure 8 as $\alpha = dE_g(x)/dx$. For the composition $Mo_{0.3}W_{0.7}Se_2$, this yields the value $\alpha \simeq 0.15 \text{ eV}$.[26] The value $m = m_e + m_h$ of the exciton mass in $MoSe_2$ and in WSe_2 is close to the free electron mass, $m \approx m_0 = 9 \times 10^{−31} \text{ kg}$,[4] the estimated concentration of lattice sites is on the order of $N \approx 10^{15} \text{ cm}^{−2} \approx 10^{19} \text{ m}^{−2}$. Substituting these values into eq 12, one obtains the dependence $\varepsilon_0^{2D}(x)$ depicted in Figure 9. It predicts $\varepsilon_0^{2D}(0.7) \approx 5$
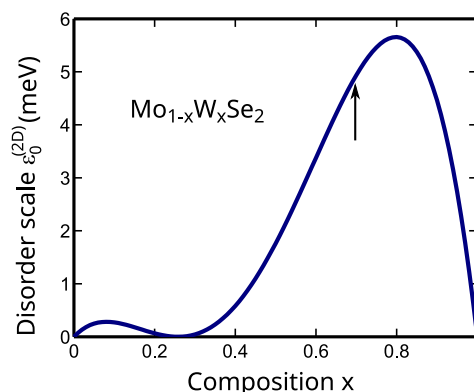
Figure 9. Composition dependence of $\varepsilon_0^{2D}(x)$ for TMD alloy $Mo_{1−x}W_xSe_2$ calculated via eqs 12, 14, and 17. The arrow corresponds to the composition $x = 0.7$ studied by Masenda et al.,[4] who revealed from experimental data the estimate $\varepsilon_0^{2D}(0.7) \approx 7 \text{ meV}$.

meV. This value is very close to the estimate $\varepsilon_0 \approx 7 \text{ meV}$ obtained experimentally[4] from the T dependences of the PL Stokes shift $\Delta_{PL}(T)$ and from the PL line width $\delta_{PL}(T)$ in the TMD alloy of composition $Mo_{0.3}W_{0.7}Se_2$.

The agreement between the estimate $\varepsilon_0 \approx 7 \text{ meV}$ from experimental study[4] and the theoretical estimate $\varepsilon_0^{2D} \approx 5 \text{ meV}$ given by eq 12 allows one to conclude that the alloy compositional disorder provides an essential contribution to the disorder potential responsible for exciton dynamics evidenced in the nonmonotonous T dependences of the PL features.[4] This conclusion means that the quality of samples used by Masenda et al.[4] is so high that the unavoidable limit of disorder due to perfectly random spatial fluctuations of the alloy composition x has been achieved.

Furthermore, the experimental estimate for ε_0 agrees with the theoretical estimate ε_0^{2D} given by eq 12 remarkably well without extra numerical factors in this equation. It probably means that eq 12 is sufficient to determine the energy scale of the alloy

disorder in 2D systems without extra numerical factors such as a constant λ in eq 9.

The latter conclusion does not exclude the presence of other disorder mechanisms in the TMD monolayers $Mo_{1-x}W_xSe_2$. The peculiar temperature dependences $\Delta_{PL}(T)$ and $\delta_{PL}(T)$ depicted in Figure 4 and exploited by Masenda et al.[4] to reveal the estimate 6.5 meV $\leq \varepsilon_0 \leq$ 8.6 meV are due to the exciton dynamics related to the tunneling transitions of excitons between the localized states in the band tails.[7−10,28] These dynamics are to be expected at high concentrations of localized band-tail states, which is the case for the alloy disorder. If, however, the concentration of localized states created by some disorder mechanism is too low to allow exciton dynamics via transitions of excitons between localized states, the peculiar features of the PL temperature dependences depicted in Figure 4 are not observed.[4]

3.3. Mixing Disorder in Organic Semiconductors.
Recently a breakthrough with respect to band structure engineering has been achieved for organic semiconductors.[5,6] First Schwarze et al.[6] have proven that the ionization energies of crystalline organic semiconductors, ZnPc and SubPc, can be continuously tuned over a wide range by blending them with their halogenated derivatives, F_4ZnPc, F_8ZnPc, $F_{16}ZnPc$, and Cl_6SubPc. Later the band-gap tuning by blending was demonstrated by Ortstein et al.[5] for oligothiophenes with dicyanovinyl end groups, designed as donors in organic solar cells, where their energy levels match the fullerene acceptor C_{60}.

A detailed analysis of the ultraviolet photoelectron spectroscopy (UPS) spectra evidenced[6] linear dependences of the HOMO energies on the fraction x of one of the components in the blends, for instance, of the ZnPc fraction in the blend $(ZnPc)_x(F_nZnPc)_{1-x}$ and of the SubPc fraction in the blend $(SubPc)_x(Cl_6SubPc)_{1-x}$. The samples were obtained by thermal coevaporation under ultrahigh vacuum at a base pressure of 10^{-8} mbar using individual quartz crystal monitors for each material.

Identifying the HOMO distribution maxima in organic semiconductors with the valence band edge, $E_v(x)$, in conventional inorganic materials, one can try to apply equations for alloy disorder derived in Section 2 to organic semiconductors. Let us try to make the corresponding estimate for the energy scale of disorder, ε_0, in the blend $(ZnPc)_x(F_4ZnPc)_{1-x}$ using eq 9. The derivative of the valence-band edge $E_v(x)$ with respect to the composition x can be estimated from the UPS data[6] as $dE_v(x)/dx \simeq 1$ eV. The concentration of sites, N, in this equation should be taken as the concentration of molecules in the organic alloy. This concentration can hardly exceed $N \simeq 10^{21}$ cm^{-3}. The effective mass, m, of charge carriers in organic crystals can hardly be smaller than the free electron mass m_0 because of the narrow bands in organic crystals, as compared to inorganic materials. Inserting the values $\alpha = dE_v(x)/dx = 1$ eV, $N = 10^{21}$ cm^{-3}, and $m = m_0$ into eq 9, one comes with $\lambda = 1$ to the estimate $\varepsilon_0 \simeq 140$ eV, which is unrealistically large for the energy scale of disorder potential.

Let us discuss possible solutions for the discrepancy between this estimate and the real spread of electron energies of about 1 eV, as can be judged from the line width in the UPS studies.[6] One might try to speculate about a possibly small value of the numerical factor λ in eq 9. So far, estimates for λ exist in the literature only for the asymptotically deep tail of the DOS in the band gap. Halperin and Lax[14] gave the value $\lambda = (18\pi^2)^{-1}$ with a reference to unpublished work. A similar value, $\lambda \simeq 1/178$, was suggested by Baranovskii and Efros.[15] In the case of the DOS $g(\varepsilon)$ given by eq 16, such estimates might be valid at $E_c - \varepsilon \gg \varepsilon_0$,

though probably not valid to determine the energy scale of disorder in the vicinity of the band edge. Taking the value $\lambda \simeq 1/178$, one comes via eq 9 to the dependence $\varepsilon_0(x)$ plotted in Figure 10a. Extending this speculation, one could compare this
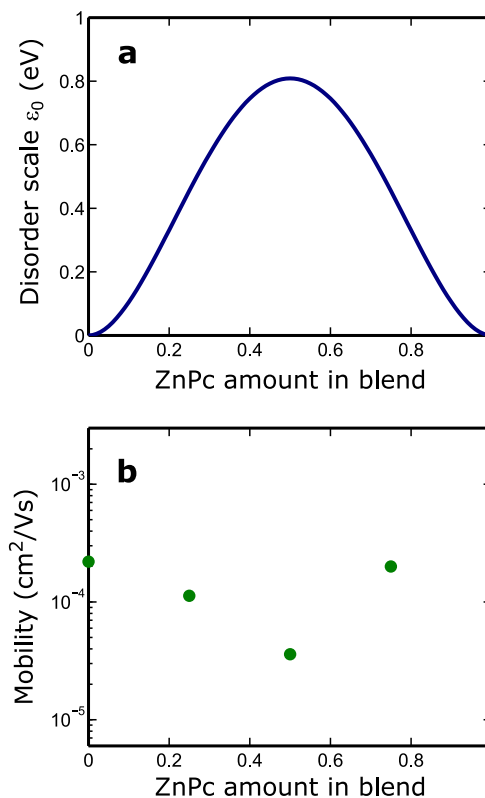
Figure 10. (a) Disorder energy scale in the blend $(ZnPc)_x(F_4ZnPc)_{1-x}$ calculated via eq 9 with $\lambda = 1/178$ and parameter values given in the text. (b) Values of the field-effect carrier mobility measured by Schwarze et al.[6] in the blend $(ZnPc)_x(F_4ZnPc)_{1-x}$. Adapted with permission from ref 6. Copyright 2016 by the AAAS.

result with the dependence of the carrier field-effect mobility $\mu(x)$ on the blend mixing ratio x measured in $(ZnPc)_x(F_4ZnPc)_{1-x}$ by Schwarze et al.,[6] as depicted in Figure 10b. The larger the $\varepsilon_0(x)$, the smaller the $\mu(x)$. This trend is to be expected in general for charge transport in organic semiconductors.[29,30] However, one should take into account that there is no sufficiently strong justification for using the small numerical factor λ in eq 9. Furthermore, the validity of eq 9 for organic semiconductors with narrow conduction and valence bands as compared to the value of parameter α can hardly be justified due to the following reason.

Let us consider for certainty a conduction band in an organic semiconductor and denote its width as W. Arguments based on physical dimensions similar to those given in Section 2 lead to the estimate for effective mass $m \simeq \hbar^2/(Wa^2)$, where $a \simeq N^{-1/3}$ is the distance between the neighboring molecules in the organic crystal. Inserting these estimates for m and a into eq 9, one comes to the estimate for the energy scale

$$\varepsilon_0 \simeq \lambda W \left(\frac{\alpha}{W} \right)^4 x^2 (1 - x)^2 \tag{18}$$

The spatial scale of alloy disorder in accord with eq 11 then has the value

$$\tilde{R} \simeq a \left(\frac{W}{\alpha}\right)^2 [x(1-x)]^{-1} \qquad (19)$$

The bandwidth W in organic semiconductors is typically smaller than 1 eV: i.e., the inequality $W < \alpha$ should hold for the blend $(ZnPc)_x(F_4ZnPc)_{1-x}$ with $\alpha \simeq 1$ eV. In such a case, the spatial scale $\tilde{R}$ of the compositional fluctuations given by eq 19 should be smaller than the distance a between the neighboring molecules. This unrealistic estimate points to the invalidity of the theory for alloy disorder developed in Section 2 for the blend $(ZnPc)_x(F_4ZnPc)_{1-x}$.

For other organic blends, the situation can be different. For instance, the HOMO peak in the blend $(SubPc)_x(Cl_6SubPc)_{1-x}$ depends on the blend mixing ratio x much more weakly than in the case of $(ZnPc)_x(F_4ZnPc)_{1-x}$.[6] Identifying this peak with the valence band edge $E_v(x)$, one comes to the estimate $\alpha_v \simeq 0.15$ eV. Inserting the values $\alpha = 0.15$ eV, $N = 10^{21}$ cm^{-3}, $m = m_0$, and $\lambda = 1$, one comes via eq 9 to the estimate $\varepsilon_0 \simeq 70$ meV, which does not look unrealistic.

Apparently, the description of the structural disorder in organic blends remains a challenge for future theoretical treatments. Very important in this respect is the theoretical analysis,[5] which shows that the tuning of the band structure in organic semiconductors can be mainly caused by a change in the dielectric constant with the blend ratio. This mechanism for tuning the band structure in organic materials deviates decisively from the mechanism based on the isoelectronic substitution of the alloy components used for the band-structure engineering in inorganic semiconductors.

4. CONCLUSIONS

The effects of the compositional disorder in alloy semiconductors have been considered theoretically. This kind of disorder is caused by statistical fluctuations in the spatial distribution of the alloy components. It is unavoidable even for the desirable case of random spatial distributions. The combinations of alloy parameters responsible for the energy and spatial scales of the disorder landscape are derived solely from the physical dimensions of the input parameters, separately for 3D and 2D systems.

The results are shown to be of high importance for 3D perovskite alloys desired for applications in modern photovoltaics. Remarkably, theory predicts that the maximum disorder effects are to be expected in alloys not necessarily with a 50:50 mixing ratio of alloy components but rather at compositions with the steepest dependence of the band structure on the mixing ratio. It explains, for instance, why Pb-rich and Sn-rich Sn−Pb perovskites typically show shorter PL lifetimes, broader emission, increased Stokes shifts, reduced PL quantum yield, and higher Urbach tails, compared with their lead-only counterparts.[3,11,20]

Theoretical results also appear valuable for 2D systems, such as alloyed transition-metal dichalcogenide monolyers desired for applications in modern optoelectronics, spintronics, and valleytronics. Theoretical results for alloy disorder in the 2D case agree with experimental data[4] showing that the low limit of disorder effects corresponding to the statistical compositional fluctuations is achieved by the modern crytal growth technology.

In contrast, a comparison between the derived theoretical results for the compositional disorder with the experimental data in organic semiconductor blends desired for band-structure engineering[5,6] seems rather controversial. Although qualitative trends in experimental data do not contradict theoretical predictions, the quantitative estimates of the energy and spatial scales of disorder potential do not provide a self-consistent picture, if they are based on the theory developed for inorganic alloys. More theoretical research is apparently needed to describe disorder effects in organic blends.

It is worth emphasizing that the presented theory provides useful information for the technological development of novel materials desired for applications. The theory developed in Section 2 gives the quantitative estimate for the lowest limit of energy disorder in alloys that arises from unavoidable statistical fluctuations in the spatial distribution of alloy components. If a manufactured material demonstrates a significantly larger energy scale of disorder than the estimates in Section 2, one could try to reduce the disorder effects by further crystal growth optimization. If, however, the energy scale of disorder potential in the manufactured material is quantitatively comparable with the estimates in Section 2, further crystal growth optimization is futile.

Furthermore, the theory developed in Section 2 provides the combination of material parameters responsible for the compositional disorder. Although this kind of disorder is unavoidable, equations in Section 2 give a hint as to the choice of materials with parameters favorable to manufacture devices with minimal disorder effects for current and future applications.

■ AUTHOR INFORMATION

Corresponding Authors

Sergei D. Baranovskii − *Department für Chemie, Universität zu Köln, 50939 Köln, Germany; Faculty of Physics, Philipps-Universität Marburg, Marburg 35032, Germany;* ⓘ orcid.org/0000-0002-0557-0665; Email: sergei.baranovski@physik.uni-marburg.de

§Alexey V. Nenashev − *Faculty of Physics, Philipps-Universität Marburg, Marburg 35032, Germany;* Email: nenashev_isp@mail.ru

Authors

Dirk Hertel − *Department für Chemie, Universität zu Köln, 50939 Köln, Germany*

Florian Gebhard − *Faculty of Physics, Philipps-Universität Marburg, Marburg 35032, Germany*

Klaus Meerholz − *Department für Chemie, Universität zu Köln, 50939 Köln, Germany*

Complete contact information is available at:
https://pubs.acs.org/10.1021/acsomega.2c05426

Notes

The authors declare no competing financial interest.
§On a leave of absence from Rzhanov Institute of Semiconductor Physics and the Novosibirsk State University, Russia.

Biographies

Sergei D. Baranovskii−Prof. Sergei Baranovskii received his Ph.D. degree (1981) in theoretical physics from Ioffe Institute in St. Petersburg, where he worked as a senior researcher until 1990. Since 1990, he has been working at the Philipps University Marburg, Germany. His research interests are devoted to the optical properties of semiconductor quantum structures and to charge transport and optical properties of amorphous organic and inorganic materials. He is the author and coauthor of more than 250 publications in international journals and of 6 book chapters and is the editor of two books.

Alexey V. Nenashev−Prof. Alexey Nenashev is a senior researcher at Rzhanov Institute of Semiconductor Physics (Novosibirsk, Russia),

where he received a Ph.D. degree in 2004. In parallel, he has a teaching activity at Novosibirsk State University, where he obtained a position of associate professor in 2010. Currently, Alexey Nenashev is a guest professor at Philipps-University Marburg (Germany). Alexey Nenashev has nearly 100 scientific publications on the electronic structire of semiconductor quantum dots and transport properties of organic semiconductors and other disordered media.

Dirk Hertel—Dr. Hertel is a research scientist in Prof. Meerholz's group at the University of Cologne. His research interests include photophysical processes in conjugated organic materials and the impact of order on the aforementioned. His favorite topic is, however, charge transport in organic matter. He obtained his doctoral degree in 2000 from the Philipps-University Marburg, spending a few years at Schott (Mainz) before moving to Cologne in 2004.

Florian Gebhard—Prof. Florian Gebhard received his doctoral degree from the RWTH Aachen, Germany, in 1990. After research stays at Rutgers University, NJ, USA, and the Institute Laue-Langevin (ILL), France, he became full professor of physics at the Philipps University Marburg, Germany, in 1998. He uses the Gutzwiller variational method to study magnetism in transition metals and their compounds and the density-matrix renormalization group (DMRG) method for the electro-optical properties of polymers. Apart from the physics of strongly correlated electron systems, he is interested in the properties of disordered semiconductor materials.

Klaus Meerholz—Prof. Klaus Meerholz studied chemistry at the Universities of Bielefeld and Freiburg, and he received his Ph.D. in 1991. He was a postdoctoral fellow at SUNY Buffalo, USA, and an Assistant Research Scientist at the Optical Sciences Center, University of Arizona, USA, (1993−1995). In 1995 he moved to the University of Munich (LMU), where he finished his Habilitation in 1998. Since 2001 he has held the Chair of Physical Chemistry at the University of Cologne/Germany. His research interests include various kinds of optoelectronic devices based on organic semiconductors such as light-emitting diodes, solar cells, memories, and batteries. Recent work addresses template-desigend organic electronics using graphene nanoribbons.

■ REFERENCES

(1) Baranovskii, S. D.; Doerr, U.; Thomas, P.; Naumov, A.; Gebhardt, W. Exciton line broadening by compositional disorder in alloy quantum wells. *Phys. Rev. B* **1993**, *48*, 17149−17154.

(2) Weisbuch, C.; Nakamura, S.; Wu, Y.-R.; Speck, J. S. Disorder effects in nitride semiconductors: impact on fundamental and device properties. *Nanophotonics* **2020**, *10*, 3−21.

(3) Parrott, E. S.; Green, T.; Milot, R. L.; Johnston, M. B.; Snaith, H. J.; Herz, L. M. Interplay of Structural and Optoelectronic Properties in Formamidinium Mixed Tin-Lead Triiodide Perovskites. *Adv. Funct. Mater.* **2018**, *28*, 1802803.

(4) Masenda, H.; Schneider, L. M.; Aly, M. A.; Machchhar, S. J.; Usman, A.; Meerholz, K.; Gebhard, F.; Baranovskii, S. D.; Koch, M. Energy Scaling of Compositional Disorder in Ternary Transition-Metal Dichalcogenide Monolayers. *Adv. Electron. Mater.* **2021**, *7*, 2100196.

(5) Ortstein, K.; et al. Band gap engineering in blended organic semiconductor films based on dielectric interactions. *Nat. Mater.* **2021**, *20*, 1407−1413.

(6) Schwarze, M.; Tress, W.; Beyer, B.; Gao, F.; Scholz, R.; Poelking, C.; Ortstein, K.; Günther, A. A.; Kasemann, D.; Andrienko, D.; Leo, K. Band structure engineering in organic semiconductors. *Science* **2016**, *352*, 1446−1449.

(7) Karcher, C.; Jandieri, K.; Kunert, B.; Fritz, R.; Zimprich, M.; Volz, K.; Stolz, W.; Gebhard, F.; Baranovskii, S. D.; Heimbrodt, W. Peculiarities of the photoluminescence of metastable Ga(N,As,P)/GaP quantum well structures. *Phys. Rev. B* **2010**, *82*, 245309.

(8) Jandieri, K.; Shakfa, M. K.; Liebich, S.; Zimprich, M.; Kunert, B.; Karcher, C.; Chernikov, A.; Volz, K.; Stolz, W.; Koch, M.; Chatterjee, S.; Heimbrodt, W.; Gebhard, F.; Baranovskii, S. D. Energy scaling of compositional disorder in Ga(N,P,As)/GaP quantum well structures. *Phys. Rev. B* **2012**, *86*, 125318.

(9) Baranovskii, S. D.; Eichmann, R.; Thomas, P. Temperature-dependent exciton luminescence in quantum wells by computer simulation. *Phys. Rev. B* **1998**, *58*, 13081−13087.

(10) Dal Don, B.; Kohary, K.; Tsitsishvili, E.; Kalt, H.; Baranovskii, S. D.; Thomas, P. Quantitative interpretation of the phonon-assisted redistribution processes of excitons in $Zn_{1-x}Cd_xSe$ quantum islands. *Phys. Rev. B* **2004**, *69*, 045318.

(11) Savill, K. J.; Ulatowski, A. M.; Farrar, M. D.; Johnston, M. B.; Snaith, H. J.; Herz, L. M. Impact of Tin Fluoride Additive on the Properties of Mixed Tin-Lead Iodide Perovskite Semiconductors. *Adv. Funct. Mater.* **2020**, *30*, 2005594.

(12) Siegner, U.; Weber, D.; Göbel, E. O.; Bennhardt, D.; Heuckeroth, V.; Saleh, R.; Baranovskii, S. D.; Thomas, P.; Schwab, H.; Klingshirn, C.; Hvam, J. M.; Lyssenko, V. G. Optical dephasing in semiconductor mixed crystals. *Phys. Rev. B* **1992**, *46*, 4564−4581.

(13) Wiemer, M.; Jandieri, K.; Koch, M.; Gebhard, F.; Baranovskii, S. D. Band edge smearing due to compositional disorder in multi-component d-dimensional alloys. *Phys. Status Solidi RRL* **2016**, *10*, 911.

(14) Halperin, B. I.; Lax, M. Impurity Band Tails in the High Density Limit. I. Minimum Counting Methods. *Phys. Rev.* **1966**, *148*, 722−740.

(15) Baranovskii, S. D.; Efros, A. L. Band edge smearing in solid solutions. *Sov. Phys. Semicond.* **1978**, *12*, 1328−1330.

(16) Alferov, Z. I.; Portnoi, E. M.; Rogachev, A. A. Width of Absorption Edge of Semiconducting Solid Solutions. *Sov. Phys. Semicond.* **1969**, *2*, 1001.

(17) Raikh, M. E.; Baranovskii, S. D.; Shklovskii, B. I. Dimensional quantization in a-Si:H quantum-well structures: The alloy model. *Phys. Rev. B* **1990**, *41*, 7701−7704.

(18) Frohna, K.; Anaya, M.; Macpherson, S.; Sung, J.; Doherty, T. A. S.; Chiang, Y.-H.; Winchester, A. J.; Orr, K. W. P.; Parker, J. E.; Quinn, P. D.; Dani, K. M.; Rao, A.; Stranks, S. D. Nanoscale chemical heterogeneity dominates the optoelectronic response of alloyed perovskite solar cells. *Nat. Nanotechnol.* **2022**, *17*, 190.

(19) Al-Ashouri, A.; et al. Monolithic perovskite/silicon tandem solar cell with above 29% efficiency by enhanced hole extraction. *Science* **2020**, *370*, 1300−1309.

(20) Klug, M. T.; et al. Metal composition influences optoelectronic quality in mixed-metal lead-tin triiodide perovskite solar absorbers. *Energy Environ. Sci.* **2020**, *13*, 1776−1787.

(21) Baranovskii, S. D.; Höhbusch, P.; Nenashev, A. V.; Dvurechenskii, A. V.; Gerhard, M.; Hertel, D.; Meerholz, K.; Koch, M.; Gebhard, F. Comment on "Interplay of Structural and Optoelectronic Properties in Formamidinium Mixed Tin-Lead Triiodide Perovskites. *Adv. Funct. Mater.* **2022**, *32*, 2201309.

(22) *Charge Transport in Disordered Solids with Applications in Electronics*; Baranovski, S., Ed; Wiley: 2006.

(23) Mak, K. F.; Xiao, D.; Shan, J. Light-valley interactions in 2D semiconductors. *Nat. Photonics* **2018**, *12*, 451−460.

(24) Avsar, A.; Ochoa, H.; Guinea, F.; Zyilmaz, B.; Wees, B. J. V.; Vera-Marun, I. J. Colloquium: Spintronics in graphene and other two-dimensional materials. *Rev. Mod. Phys.* **2020**, *92*, 021003.

(25) Schaibley, J. R.; Yu, H.; Clark, G.; Rivera, P.; Ross, J. S.; Seyler, K. L.; Yao, W.; Xu, X. Valleytronics in 2D materials. *Nat. Rev. Mater.* **2016**, *1*, 16055.

(26) Zhang, M.; Wu, J.; Zhu, Y.; Dumcenco, D. O.; Hong, J.; Mao, N.; Deng, S.; Chen, Y.; Yang, Y.; Jin, C.; Chaki, S. H.; Huang, Y. S.; Zhang, J.; Xie, L. Two-dimensional molybdenum tungsten diselenide alloys: Photoluminescence, Raman scattering, and electrical transport. *ACS Nano* **2014**, *8*, 7130−7137.

(27) Raja, A.; Waldecker, L.; Zipfel, J.; Cho, Y.; Brem, S.; Ziegler, J. D.; Kulig, M.; Taniguchi, T.; Watanabe, K.; Malic, E.; Heinz, T. F.; Berkelbach, T. C.; Chernikov, A. Dielectric disorder in two-dimensional materials. *Nat. Nanotechnol.* **2019**, *14*, 832−837.

(28) Shakfa, M. K.; Jandieri, K.; Wiemer, M.; Ludewig, P.; Volz, K.; Stolz, W.; Baranovskii, S. D.; Koch, M. Energy scale of compositional disorder in Ga(AsBi). *J. Phys. D: Appl. Phys.* **2015**, *48*, 425101.

(29) Baranovskii, S. D. Theoretical description of charge transport in disordered organic semiconductors. *Phys. Status Solidi B* **2014**, *251*, 487.

(30) Baranovskii, S. D. Mott lecture: Description of charge transport in disordered organic semiconductors: Analytical theories and computer simulations. *Phys. Status Solidi A* **2018**, *215*, 1700676.